Adsorption of Poly(methyl methacrylate) Melts on Quartz

C. J. Durning,* B. O'Shaughnessy, and U. Sawhney†

Department of Chemical Engineering and Applied Chemistry Columbia University, New York, New York 10027

D. Nguyen

PPG Industries, Inc., R&D Center, Allison Park, Pennsylvania 15101

J. Majewski and G. S. Smith

Los Alamos National Laboratory, Los Alamos, New Mexico 87545

Received November 17, 1998; Revised Manuscript Received June 28, 1999

ABSTRACT: We studied by neutron reflection the architecture of poly(methyl methacrylate) (PMMA) layers adsorbed on hydroxylated quartz from the melt. The samples were prepared by spin-coating about 1 μm thick films of PMMA onto quartz plates, annealing at melt conditions for an extended period, and then leaching away unbound material in good solvent (benzene). Data on dry residual layers indicated a dense PMMA layer the thickness of which gradually increased with annealing time in the melt from an initial minimal value toward a final equilibrium thickness. Evidently, annealing in the melt gradually relaxes the rather flat nonequilibrium structure produced by spin-coating. The thicknesses, h, in a series of dry residual layers annealed for very long times in the melt obey $h \sim N^{0.47\pm.05}$, where N is the degree of polymerization. This is close to the scaling expected for a reflected random walk (RRW) immobilized by the surface ($h \sim N^{1/2}$). Data on residual adsorbed layers swollen in a good solvent (deuterated benzene) indicate a strongly stretched, brushlike structure with a diffuse segment density profile, $\phi(z)$. The segment density decays $\phi(z) \sim z^{-0.77\pm.03}$, faster than predicted by RRW statistics and indicates fewer long loops per chain than the RRW model.

I. Introduction

Polymers physisorb so strongly onto solids that the attachment often seems irreversible. It is a result of the large number of direct segmental contacts per chain, which makes the energetic penalty per chain for desorption very high. This strong interaction affects a number of practical applications involving contact between melts and solids, including melt processing operations and composite fabrication. Despite the practical importance, the majority of prior work focuses on adsorption from dilute solution; there are relatively few basic studies of adsorption from melts or concentrated solutions. In this work, we characterize the structure of layers adsorbed from the melt onto smooth, flat solids under well-controlled contacting conditions.

A. Equilibrium Architecture. The equilibrium structure of a melt at an inert, solid wall has been studied by mean-field models. deGennes[1] examined a single chain in a monodisperse melt against a flat, impenetrable wall by a self-consistent field method. The wall's effect is screened beyond distances on the order of the monomer size, so essentially reflecting random-walk statistics[2] are maintained. This has a number of simple consequences. For example, at equilibrium an "adsorbed" chain[3] of N segments makes on the order of $N^{1/2}$ contacts and has the loop distribution $f(n) \sim N^{1/2}n^{-3/2}$, where n is the number of segments in a loop;[4] at the same time the "coverage", Γ (the total number of segments belonging to adsorbed chains, per unit area of wall), obeys $\Gamma \sim N^{1/2}$. What happens when short-ranged attractive interactions between the segments and the wall are switched on? The lattice mean-field model by Schuetjens and Fleer,[5] as well as lattice Monte Carlo calculations on many-chain systems,[6] indicates that single-chain statistics with and without surface attraction are essentially identical. It suggests that the interfacial architecture of melts at equilibrium near a wall is independent of the local-scale chemistry of both the chains *and* the surface.

Experimental verification of this strong prediction is difficult. First, in situ examination of single chains adsorbed from the melt, or of the whole adsorbed layer, requires some sort of contrast between adsorbed and unbound material. Inevitably, one has to contact the melt and solid and then strip or replace unbound material to examine the bound layer; to do so *without* drastically altering the structure at the wall is a considerable challenge. It requires that the adsorbed layer be robust to removal of unbound material by a solvent, i.e., that the barrier for segmental desorption against solvent be relatively high, at least $\gtrsim O(kT)$. At the same time, one has to reproducibly establish the interfacial equilibrium between the melt and solid after first contact; for robustly bound layers this certainly involves a protracted relaxation of the interfacial structure after first contact, a process which is poorly understood at present.[7]

Despite such difficulties, a few experiments have succeeded to provide a modicum of support for the reflected random-walk picture. Cohen-Addad[8] studied poly(dimethylsiloxane) (PDMS) melts on silica particles; the weight of polymer adsorbed per unit mass of silica was measured after contacting with the melt, waiting, and finally rinsing away unbound material in a carefully

* To whom correspondence should be sent.
† Present address: Department of Chemical Engineering, Indian Institute of Technology, New Delhi 110016, India.

10.1021/ma981785k CCC: $18.00
Published on Web 09/18/1999

chosen solvent. This system is complex, involving polydisperse polymer ($M_w/M_n \geq 1.2$) adsorbed on irregular porous particles and showing long-lived aging effects after first contact.[9] Nonetheless, Cohen-Addad found that the absorbance (adsorbed mass per unit area, $\sim\Gamma$) scaled with $M_n^{1/2}$ with M_n being the number-average molecular weight of the PDMS, in agreement with the reflected random-walk model. Auvray et al.[10] confirmed this result on the same system by small angle neutron scattering.

B. Guiselin's Brush. Guiselin[11] derived results consequent to the reflected random-walk model for melts in contact with a neutral wall. For an equilibrated melt against an inert wall, Guiselin imagined suddenly fixing those segments in contact with the wall. He showed theoretically that after removal of unbound material and swelling of the residual bound layer in a good solvent, a brush-like[12] structure results with height $h_{swollen} \sim N^{5/6}$ and segment density profile $\phi(z) \sim z^{-2/5}$, where z denotes the distance away from the substrate. This swollen layer is much more extended than layers adsorbed from dilute solution, because of the high areal density of long loops immobilized on the surface, a remnant of the equilibrium melt architecture at the surface. Of course the *dry* residual film has the height $h_{dry} \sim N^{1/2}$ since $h_{dry} \sim \Gamma \sim$ the adsorbed mass per unit area.

Guiselin's thought experiment is ingenious but difficult to achieve in practice. In principle, one has to equilibrate the melt or dense solution against an inert solid surface and then, by some means, suddenly and permanently fix *only* the segments currently adsorbed. All experiments so far involve attractive solid surfaces, with a large barrier to segmental desorption always in force, even during initial contact between the solid and the melt. Here, one has to first equilibrate the melt with the solid after contact, which may take a long time, and then rely on the slow response of the bound layer in order to "quickly" remove unbound material and examine the structure before any significant reorganization occurs. Nonetheless, experimental verification of a "Guiselin brush" provides a demanding check of random-walk statistics for adsorbed melts. The structure is of technological interest in its own right, since it resembles a grafted brush (e.g. ref 13) important in surface modification of solids, but does not require special polymers (e.g. diblocks).

Despite the experimental difficulties, Auvray et al.[14] verified $h_{swollen} \sim N^{0.8}$ for adsorbed layers of PDMS melt on porous silica swollen in dichloromethane, using small angle neutron scattering. Their results also suggested diffuse segment density profiles, but the power-law signature for a Guiselin brush, $\phi(z) \sim z^{-2/5}$, was not verified unambiguously.

C. Nonequilibrium Architectures. If a significant barrier [at least $O(kT)$] to segmental desorption is always present, initial contact almost certainly produces a nonequilibrium structure which gradually relaxes. If the relaxation is slow enough, one can examine the transient structures at the interface by "quickly" rinsing unbound material away and examining the bound layer. We are aware of only one systematic study of this type on melts.[15,16]

In this work, we study the architecture of poly(methyl methacrylate) (PMMA) layers adsorbed on hydroxylated quartz (SiO_2) after spin-casting relatively thick films ($\simeq 1\ \mu$m) from solution in benzene, drying, and then annealing at melt conditions. In the PMMA/quartz/benzene system, we expect the differential segmental sticking energy to be fairly large (several kT),[17] so the associated barrier to segmental desorption with benzene present is likely at least $O(kT)$. Consequently, spin-casting of PMMA from benzene onto quartz should produce a strongly bound adsorbed layer with a nonequilibrium structure. The spin-cast film is dried of solvent relatively quickly[18] and then annealed for a much longer time scale at melt conditions to relax the structure at the solid−melt interface. Because the spin-cast films are relatively thick, the adsorbed layer at the interface relaxes in contact with a large reservoir of unattached chains. Consequently, during annealing the coverage can change; for example, initially unattached chains can adsorb during the interfacial relaxation by replacement of segments at surface sites. After a fixed annealing time, subsequent cooling to below the glass transition temperature freezes in the interfacial structure, and rinsing with benzene removes unadsorbed polymer while imposing a high barrier against desorption of segments, preventing reorganization of bound chains. Consequently, we are able to observe transient, nonequilibrium structures immobilized at the interface. When annealed long enough, the interface architecture equilibrates. In principle, long enough annealing in the melt, followed by rinsing and swelling of the residual bound material, should result in a Guiselin brush.

In what follows we first explain the experimental methods in more detail; neutron reflection is our main technique for analyzing the bound layers. Following that, we summarize preliminary theoretical calculations predicting the appearance of reflectivity data, based on crude "box" models for the adsorbed structures anticipated; these are particularly helpful in understanding the data on adsorbed layers swollen in good solvent. The next section presents experimental data on dry, residual layers. We find that without annealing the melt before cooling to below the glass transition and stripping unbound material, very thin (10−20 Å) dense layers result, independent of polymer molecular weight. With annealing, the residual layer thickens and eventually reaches an equilibrium, molecular-weight-dependent depth. In the final section, we discuss data revealing the structure of swollen layers resembling Guiselin's brush.

II. Experimental Section

A. Materials. Nearly monodisperse PMMAs with molecular weights ranging from 13K to 1200K were obtained from Polymer Laboratories Inc. (Amherst, MA) and Polymer Source Inc. (Dorval, Quebec, Canada). Table 1 shows the molecular weights and polydispersities according to the manufacturers. Polymer Laboratories specified the tacticity of their polymers as 53% syndiotactic, 40% atactic, and 7% isotactic; Polymer Source specified their product as being 75−80% syndiotactic.

Single-crystal blocks and fused quartz disks were obtained from Heraeus Amersil Inc. (Duluth, GA) and polished by Virgo Optics (Port Richey, FL). Heraeus specified the quartz as having variations in refractive index $\Delta n \leq 10^{-6}$. The polishing specifications are as follows: long-range waviness less than $\lambda/4$; surface quality better than 10/5 (scratch/dig).

To prepare polymer solutions for casting, and as the leaching solvent, HPLC grade and ACS reagent grade benzene were used. Deuterated benzene (C_6D_6; D-benzene), obtained from Cambridge Isotope Laboratories, was 99.6% pure and used in experiments designed to probe the structure of swollen adsorbed layers. Heavy water (D_2O, 99.9% pure) was also

Table 1. Molecular Weights of Poly(methyl methacrylates)

molecular weight ($M_n \times 10^{-3}$)	polydispersity (M_w/M_n)
13[a]	1.05
25[a]	1.05
60[a]	1.05
100[a]	1.05
1200[a]	1.04
13.8[b]	1.03
70.9[b]	1.14
174[b]	1.04
216[b]	1.05
345[b]	1.15
520[b]	1.06
1232[b]	1.15

[a] Obtained form Polymer Laboratories, LTD,; manufacturer supplied glass transition was 110 °C. [b] Obtained from Polymer Source, Inc.; manufacturer supplied glass transition 127−134 °C.

obtained from Cambridge Isotope Laboratories, and used in some experiments to study the structure of dry, residual adsorbed layers.

B. Substrate Preparation. Before contacting, the quartz substrates were cleaned and hydroxylated by a protocol which gave reproducible results in subsequent surface characterizations by neutron reflection and water contact-angle measurements. First, the substrates were immersed in aqua regia (3:1 hydrochloric:nitric acid) for 4−6 h, followed by rinsing with Millipore filtered, deionized (18.2 MΩ) water, followed by UV−ozone plasma oxidation for 120 min. This procedure effectively removes organic contaminants. This was followed by immersion in concentrated hydrochloric acid for 2 h to hydroxylate the surface. The surface was finally rinsed with Millipore filtered, deionized (18.2 MΩ) water to yield a clean hydrophilic surface. According to the literature,[19−21] fused silica powders subject to this surface treatment get surface hydroxyl densities on the order of 0.01−0.1 Å^{-2}; we expect that a similar surface chemistry results for the single surfaces used here. Neutron reflection on freshly cleaned surfaces always gave a nearly Fresnel response (see subsequent discussion), indicating that the oxidation steps indeed removed organic surface contaminants. Water contact-angle measurements gave consistently low contact angles (below 15°), indicating significant surface hydroxylation and hydrophilicity of the surface.

C. Adsorbed Layer Formation. Moderately concentrated solutions (10−20 wt %) of PMMA in benzene were prepared by slow stirring of the as-received polymer in warm solvent (≈40 °C) for 24−48 h. The solution was then spun onto the quartz at 2000−3000 rpm to produce thin coatings approximately 1 μm in thickness. Then, the coated samples were annealed at 165 ± 1 °C in an argon purged oven for various lengths of time.[22] The annealing step drives off residual casting solvent and liquefies the overcoating of PMMA, allowing the melt to equilibrate against the hydroxylated quartz surface. The annealed samples were then cooled to room temperature and subsequently leached three times in baths of benzene. Each leach was for approximately 3 h and concluded with 5−10 min of ultrasonication to aid the stripping of the unbound material. Finally, the sample was either dried on a hot plate (70−80 °C) to remove traces of benzene from the adsorbed layer and analyzed against air or D_2O or immediately contacted with D-benzene in a sealed cell similar to that described in ref 23.

D. Specular Neutron Reflection. The technique involves directing a collimated neutron beam onto a flat interface at low incidence angle, θ, and measuring the ratio of reflected to incident intensity, R, as a function of momentum transfer $q = 4\pi \sin \theta/\lambda$, where λ is the neutron wavelength. We only consider cases where the lower medium has a higher scattering length density than the upper. Then, $R = 1$ for q below a critical value $q_c = 4\sqrt{\pi\Delta\beta}$, where $\Delta\beta$ is the scattering length density difference between the lower and upper media. Above q_c, R generally decays with q; the details depend on the (area-averaged) scattering length density profile normal to the interface. We varied q from below to well above q_c by manipulating λ and/or θ. Analyzing R vs q allows one to extract the interfacial scattering length density profile, $\beta(z)$.

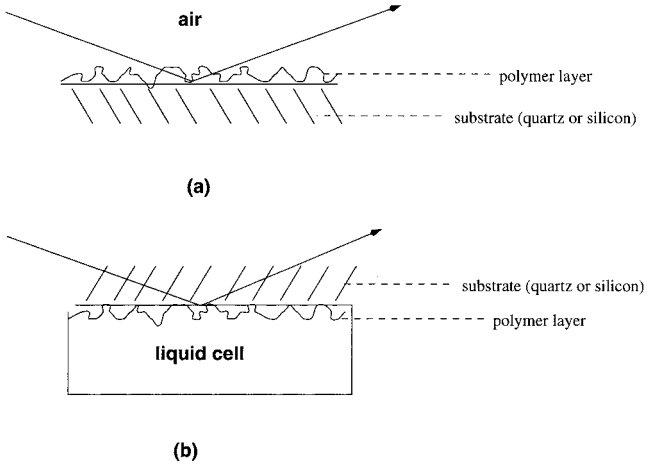

Figure 1. Schematic of experimental setup: (a) Upright geometry used for analysis of dry layers against air and (b) inverted geometry used for analysis of dry layers against heavy water or swollen layers against D-benzene.

The majority of experiments were performed on the SPEAR reflectometer at the Los Alamos Neutron Science Center (LANSCE), Los Alamos, NM, and some were performed at the High Flux Beam Reactor H9A′ reflectometer at the Brookhaven National Laboratory, Upton, NY. To interrogate the structure of dried residual layers, reflection was performed in "upright" geometry, with the quartz on the bottom against air above; a few experiments on dried layers were also performed in "inverted" geometry in a sealed cell, with D_2O on the bottom against quartz above (see Figure 1). Experiments to interrogate adsorbed layers swollen in D-benzene also employed inverted geometry. The inverted geometry is necessary to avoid passing the neutron beam through liquid, where the attenuation is unacceptably large; this requires deuterated fluid to provide the critical edge.

SPEAR is a time-of-flight reflectometer employing a polychromatic, pulsed neutron source. To achieve the widest range of q, two different θ were typically used for each run; data from low and high angle runs always had a substantial range of q in common and were overlapped to obtain the complete R vs q profile. Typical measurement times were 1−2 h for upright geometry and 5−10 h for inverted geometry. Uncertainties in q and R are defined by the detector's temporal and spacial resolution, the pulse width, and the total neutron counts. Estimates of these uncertainties are included in the reduction of raw data to R vs q, supplying realistic error bars for both. Data displayed subsequently show only the uncertainties in R.

The H9A′ reflectometer at Brookhaven measures the reflected intensity of a monochromatic ($\lambda = 4.16$ Å), continuous neutron beam. Here, a range of q through q_c is probed by changing the angle of incidence systematically, while a constant beam footprint is maintained on the sample. Measurement times on H9A′ were typically 2−3 times those for SPEAR. The main source of error arises from the statistical fluctuations in detector counts at a fixed incident intensity.

E. Analysis of Reflection Data. We used the dynamical theory of specular reflection,[24] neglecting absorption effects, for analysis of data. While $R(q)$ for any given $\beta(z)$ may be calculated, the inverse problem has no unique solution. We therefore used a deductive approach in analyzing the data. First, calculations were done for each situation of interest using simple "box" models, to anticipate plausible $\beta(z)$. Then, optimal values of parameters in the simplest possible box model were found by a weighted, least-squares fitting algorithm.[25] If warranted, refinements of the initial model were then explored.

We accounted for roughness at interfaces in the fits as follows. Substrate roughness was determined by fitting data on clean substrates to a Fresnel edge prediction attenuated

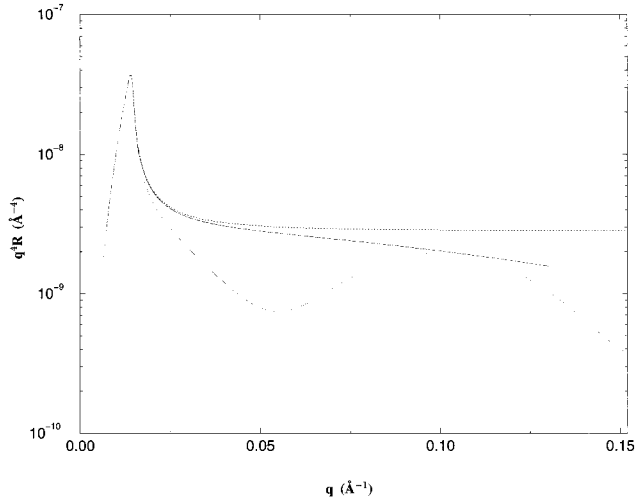

Figure 2. Calculated reflectivity curves, q^4R vs q, for single-crystal quartz against air: Flat interface (dotted line); interface with 6 Å roughness (solid line); interface with a 60 Å layer of PMMA ($\beta = 1.04 \times 10^{-6}$ Å^{-2}) and 6 Å roughness at both top and bottom interfaces (dashed line).

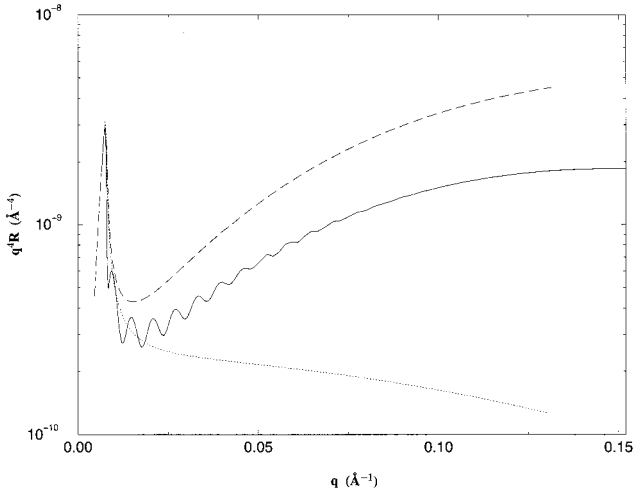

Figure 3. Calculated reflectivity curves, q^4R vs q, for single-crystal quartz against D-benzene: Interface with 6 Å roughness (dotted line); roughened interface with a single 10 Å thick hydrogenous (PMMA) layer ($\beta = 1.04 \times 10^{-6}$ Å^{-2}) (dashed line); roughened interface with the same 10 Å hydrogenous layer and an additional 1000 Å thick layer, with β corresponding to 95% D-benzene and 5% PMMA (solid line).

by a Gaussian damping function,[24] $R \rightarrow R \exp(-q^2\sigma_{substrate}^2)$, to determine $\sigma_{substrate}$, which was then considered fixed in subsequent analysis of data with adsorbed layers. In fitting data with adsorbed layers, a Gaussian damping function with an adjustable σ was applied to the reflectance for some interfaces other than that at the substrate, depending on the model chosen for that case. It should also be noted that, in all cases, the normalization for the measured intensities was treated as an adjustable parameter in the fitting of data.

Before discussing results, we summarize a few predictions for R vs q from simple box models of the situations of interest: thin, dry PMMA films on quartz against air or heavy water, and thin PMMA films swollen in D-benzene against pure D-benzene. Dry PMMA layers in the range 50−200 Å thick are considered, since this is the range of values found experimentally. These calculations motivate selection of minimal models in subsequent data analysis.

Figure 2 shows calculations for quartz against air in upright geometry. The results are plotted as q^4R vs q to highlight the deviations from the response of a Fresnel curve (dotted line), where q^4R = a constant at high q (Porod's law). The sharp peak at low q locates the critical edge, q_c, which depends only on the scattering length density difference between the adjacent media. Roughness $\sigma_{substrate}$ exponentially reduces the intensity beyond the scale $q > 1/\sigma$ (solid line). A single, thin PMMA layer on top of the rough surface puts oscillations in the profile from the interference of reflections from the top and the bottom interfaces. The fringe width gives the layer thickness. Notice that, in this system, the reflectivity of the coated substrate is always *lower* than that for the corresponding Fresnel curve, for large q. This results when the scattering length density of the film [β(PMMA) = 1.04×10^{-6} Å^{-2}] is *intermediate* between those of the adjacent media [β(air) ≪ 10^{-6} Å^{-2} and β(quartz) = 4.2×10^{-6} Å^{-2}].

Similar calculations for quartz against heavy water in inverted geometry show that the reflectivity curves with a thin, dry intervening PMMA film lie *above* the Fresnel, in contrast to the result for quartz against air (Figure 2); this occurs when β of the layer lies *below* that of either adjacent media [β(quartz) = 4.2×10^{-6} Å^{-2} and $\beta(D_2O) = 6.38 \times 10^{-6}$ Å^{-2}], creating a "well" in the β profile. The response is qualitatively the same if β for the layer lies *above* that of either adjacent media.

Finally, consider a crude model for a Guiselin brush. Theory gives $\phi(z) \sim z^{-2/5}$, which falls very quickly from the value at the substrate to much lower values and then decays very slowly with z. A crude approximation is a two-box profile, with a thin layer near the substrate comprised mainly of polymer and another much thicker layer with a much lower volume fraction of polymer. Figure 3 shows predictions from such a model designed to simulate a Guiselin brush from PMMA melt adsorbed on quartz swollen in D-benzene: A thin (10 Å) hydrogenous layer with β that of dry PMMA at the roughened interface between quartz and D-benzene, together with the effect of an additional thick layer (1000 Å) adjacent to the D-benzene with β corresponding to 95% by volume of D-benzene and 5% PMMA. The effect of the thin, hydrogenous layer alone (dashed line) is to cause a gradual rise in q^4R *above* the clean surface profile (dotted line) for $q < 0.15$ Å^{-1}, corresponding to the beginning of a very broad fringe. The thick, dilute layer suppresses the reflectivity and leads to high-frequency fringing at much lower q values. The suppression of R caused by the dilute layer can force q^4R to dip *below* the Fresnel curve at low q, since its scattering length density lies *intermediate* between those of quartz and D-benzene. Manipulating the parameters in the model shows that the gradual ascent at large q in the profile is extremely sensitive to the thickness of the thin, hydrogenous layer adjacent to the surface, which supplies a scattering length density "well" immediately next to the substrate; it is quite insensitive to variations in the thick, dilute layer's dimension and density. The general suppression of q^4R and the amplitude of the high frequency fringes depend sensitively on the weak contrast between the thick, dilute layer and the underlying D-benzene. The thick layer's dimension only affects the period of high-frequency fringing. These rough calculations provide a clear basis for interpreting data on swollen layers.

III. Results and Discussion

A. Clean Surfaces. The cleaned, functionalized quartz surfaces are extremely hydrophilic; for example, water contact angles after the surface preparation were immeasurably low. The silanol (Si−OH) density is expected to be in the range of 0.01−0.1 Å^{-2} based on estimates in the literature for powdered silica treated similarly.[20,21] The substrates were also very flat; Figure 4 shows representative reflectivity data for single-crystal surfaces after cleaning and functionalization, against air and D_2O. Very similar results were found for fused quartz substrates. Least-squares fits of the data (solid lines), letting the substrate roughness, $\sigma_{substrate}$, and quartz scattering length density, β_{qz}, vary, gave consistent values of $\sigma \simeq 6-8$ Å for both single crystal and fused-quartz and values for β_{qz} consistent with values calculated for quartz. The sharp peaks in Figure 4

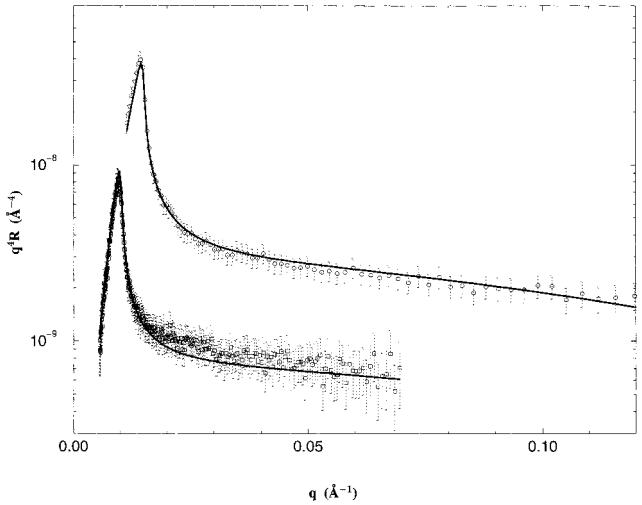

Figure 4. Typical reflectivity profiles for the bare single-crystal quartz plotted q^4R vs q: Quartz against air (circles) and quartz against heavy water (squares). The lines are fits with about 6 Å roughness.

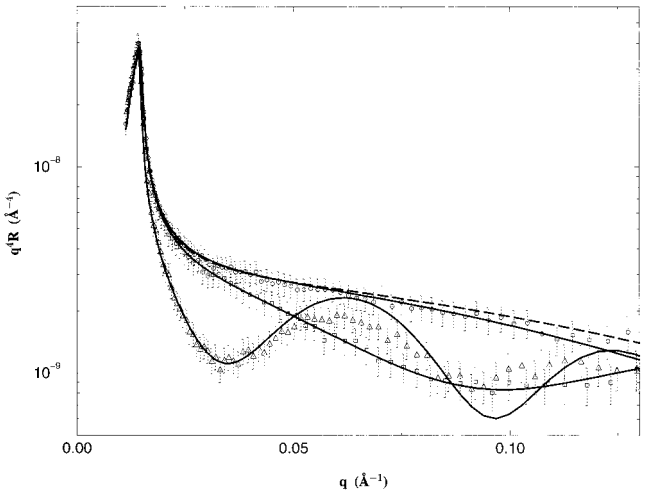

Figure 5. Reflectivity profiles, q^4R vs q, for 345 K PMMA layers on single-crystal quartz against air for different annealing times: 0 h (circles), 18 h (squares), and 108 h (triangles). Bold lines are fits with single-box models; dashed line shows fit for the clean edge against air.

indicate the critical edge, q_c, which is a function only of the scattering length density difference between the two media involved. This peak position coincided for all measured curves in a given system and showed good agreement with the theoretical value[26] in all cases. The values $\sigma_{substrate}$ and β_{qz} extracted from analyses of the clean substrates were used later as fixed constants in the analysis of data on substrates with adsorbed layers.

B. Dried, Adsorbed Layers. Recall the procedure used to produce adsorbed layers. A relatively thick film is spin-coated from moderately dense solution onto a silanol-bearing quartz surface and then dried and annealed at melt conditions; then, the annealed layer is cooled to room temperature, and unbound material is leached away in good solvent (benzene). The residual, adsorbed layer presumably corresponds to the first layer of the melt in direct contact with the surface, immobilized by cooling and rinsing.

1. Effect of Annealing Time. Consider first data on residual, adsorbed layers, dried and analyzed against air, as a function of the annealing time in the melt for a fixed molecular weight, M. Figure 5 shows the results for $M = 345$ K on single-crystal quartz. The general appearance of data agrees with predictions in Figure 2: $R(q)$ shows fringes and lies below the Fresnel curve result, indicating a film with β intermediate between those of the bounding media, i.e., $0 < \beta < 4.2 \times 10^{-6}$ Å^{-2}, characteristic of a hydrogenous layer. One sees a progressive narrowing of the fringe width with increased annealing time, indicating a gradual thickening of the residual film. Figure 6 summarizes the results for the dry residual layer thickness, h_{dry}, from single-box model fits of data against air for two molecular weights, one at either end of the range studied. Single-box model fits of dry residual films against heavy water, a nonsolvent for PMMA, using inverted geometry, gave essentially the same results for molecular weights in the same range.

For both molecular weights, a very thin layer ($\simeq$10 Å) results from spin-casting alone, without subsequent annealing, far thinner than expected from a random walk, for either molecular weight. For example, for the 70 K molecular weight, assuming each repeat unit corresponds to a Kuhn length a, $N \simeq 700$ and $a \simeq 3$ Å. This gives $R_g = N^{1/2}a/\sqrt{6} \simeq 33$ Å for a random-walk

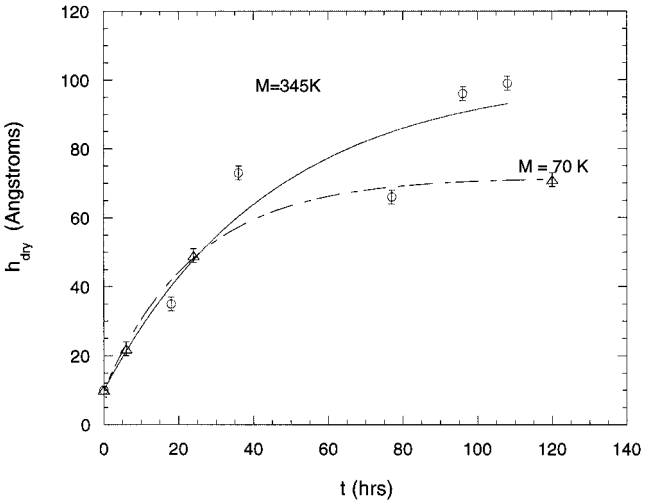

Figure 6. Dry residual adsorbed layer thickness, h_{dry}, against annealing time, t: $M = 345$ K (circles) and $M = 70$ K (triangles). The lines are exponential fits, which gave time constants 90 and 22 h, for $M = 345$ K and 70 K, respectively.

chain. Taking the Kuhn length of PMMA to be roughly three monomers increases this value to 57 Å.

The extremely small thicknesses after just spin-coating can be explained by initial contact of the polymer with the surface under solution conditions, rather than under melt conditions. In this situation, one expects that a large number of adsorption sites are not immediately covered with polymer after initial contact. Subsequent collapse of initially formed loops onto the surface to fill the vacant sites would result in a layer flat relative to the random-walk picture. This is consistent with the recent simulations of strong adsorption from dense solutions in a good solvent, carried out by Zajac and Chakrabarti.[27] They simulated suddenly activating strong but reversible segmental binding for a large reservoir of dense solution (polymer fractions up to 0.2) initially equilibrated against an inert wall. Here, not only do the segments on the surface at $t = 0$ get strongly bound but so do additional segments, which diffuse to the surface for $t > 0$. The extra adsorption for $t > 0$ changes the interfacial architecture away from a (coarse-grained) reflected random walk.

Zajac and Chakrabarti found that the extra adsorption proceeds in two stages. First, loops on chains initially in contact collapse onto the surface to fill empty sites, as described above. Then, further increases in coverage occur by a mechanism similar to end grafting, involving stretching of unattached chains to the surface and attachment by filling the few unoccupied sites, or by segmental exchange at filled sites on the surface. This process is logarithmically slow and progressively adds to the population of long tails in the adsorbed layer. Clearly the adsorbed layer produced by this process does not correspond exactly to that imagined by Guiselin. After times long enough to include tails, Zajac and Chakrabarti found that the resulting adsorbed layer shows the scaling $h_{\text{swollen}} \sim N^{0.81}$, in rough agreement with Guiselin's prediction for melts $h_{\text{swollen}} \sim N^{5/6}$; however, significant deviations are seen from the predictions $h_{\text{dry}} \sim \Gamma \sim N^{1/2}$ ($\Gamma \sim N^{0.38}$ was found) and $\phi(z) \sim z^{-2/5}$ (the simulated profile was not consistent with a power law but was closer to a displaced, flattened parabola). This work suggests that the flat architecture resulting immediately after spin-coating in our system may correspond to that simulated by Zajac and Chakrabarti before significant tail formation occurs. It is also possible that the hydrodynamics of spin-coating contributes to constructing initially flat layers: Large shear forces are involved which could stretch chains in a way that leads to in-plane orientation, and relatively flat adsorbed configurations.[28]

Returning to the data in Figure 6, one sees a gradual increase in h_{dry} with annealing time, toward a value quantitatively consistent with that for the first layer of an equilibrated melt against a wall, according to the reflected random-walk model. Time scales for equilibration, τ_{eq}, were extracted by assuming exponential relaxation of the layer thickness toward its final value. These values increase with molecular weight; assuming a power-law dependence, we get $\tau_{\text{eq}} \sim M^{0.9}$ from the results in Figure 6. While the mechanism controlling this relaxation is not at all clear, the relatively weak molecular weight dependence of τ_{eq} suggests that reptative motion is *not* involved.

2. N-Dependence of Final Thicknesses. The data in Figure 6 establish the annealing time at 165 °C needed to erase the effect of spin-casting and to equilibrate a bulk PMMA melt against the surface. Presumably, residual layers retained after annealing beyond this time scale correspond to immobilized, reflected random walks. To check this we prepared a series of residual layers annealed for relatively long times, with molecular weights ranging from 13 K to 1200 K. The dried, residual layers were analyzed against air or D_2O; the h_{dry} values were determined by fitting a one-box model to the data. In these fits, the roughness, $\sigma_{\text{substrate}}$, and the quartz scattering length density, β_{qz}, were set from the corresponding clean-edge measurement; the fitting procedure optimized the normalization, the layer's scattering length density, β, and its thickness h_{dry}. The results are collected in Table 2. For molecular weights above 60 K, the β values indicate dense PMMA layers, since they compare well with the value expected for bulk PMMA (1.04×10^{-6} Å^{-2}).

Figure 7 shows a log−log plot of h_{dry} against the degree of polymerization, N. The hollow symbols indicate samples annealed long enough for equilibration of the melt against the substrate, according to the results in Figure 6; filled symbols indicate samples that were annealed for times shorter than that anticipated for equilibrium. In the range $250 \le N \le 2160$ (25 K $\le M \le$ 216 K), a regression analysis of the data gives the scaling $h \sim N^{0.47\pm.05}$. In this range, the data agrees with $h_{\text{dry}} \sim N^{1/2}$, in accordance with the reflected random-walk picture, suggesting we have indeed achieved equilibrium melts against the surface and effectively immobilized the melt structure by cooling to below T_g and rinsing in good solvent. Figure 7 also indicates a clear failure of the $h_{\text{dry}} \sim N^{1/2}$ law for the filled symbols, corresponding to the lowest (13 K) and the highest (1200 K) molecular weights. The reason for this at the highest molecular weight is clear. Two samples were used, one annealed for 48 h and the other for 72 h; clearly, too short a time was used to equilibrate the 1200 K melt at the quartz surface (τ_{eq} for 345 K was found in to be 90 h). It appears that the annealing time used for the 345 K polymer, 108 h, was only marginal for equilibration.

For the lowest molecular weight, the dry residual layer gave an anomalously low scattering length density (see Table 2). We conjecture that this is due to patchy desorption during the leaching step, leaving a partially covered surface. Indeed, one can estimate from the surface hydroxyl density[21] and the reflected random-walk model for the adsorbed chains that, at this low molecular weight, each adsorbed chain has only on the order of 1−10 adsorption points, so significant desorption during the leaching step is plausible. Data and box-modeling for a 13 K PMMA layer against D_2O indicated a surface layer with β considerably *higher* than that of

Table 2. Results from One-Box Model Fits of Reflection Data on Dry Residual Layers after Long Annealing Times

mol. weight ($\times 10^{-3}$)	annealing (h)	h_{dry} (Å)[b]	β (Å$^{-2} \times 10^6$)
13	24	13 ± 1.0	0.66
25	52	29 ± 0.8	0.83
25[a]	24	30± 0.6	
60[a]	8	69 ± 0.6	
70	120	71± 1.2	1.15
100	120	67 ± 0.3	1.09
175	135	103 ± 2.0	0.949
216	120	115 ± 1.9	0.966
345	108	100 ± 1.1	0.901
520	181	128 ± 3.0	0.915
1200	72	36 ± 0.6	0.844
1200[a]	48	33 ± 0.8	0.890

[a] Samples observed against D_2O. [b] Uncertainties correspond to 95% confidence limits determined from the least-squares fits.

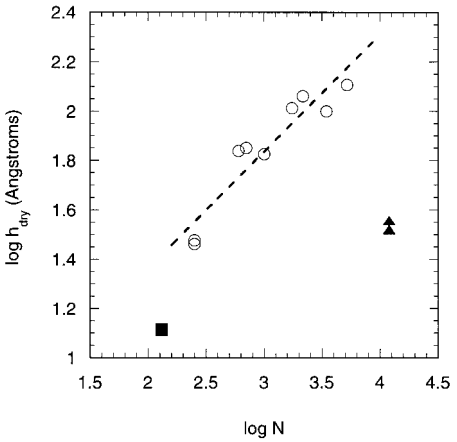

Figure 7. log−log plot of the dry residual layer height, h_{dry}, against degree of polymerization, N, for samples annealed for long times. The dashed line is the regression result of data with hollow symbols and has a slope of 0.47 ± 0.05.

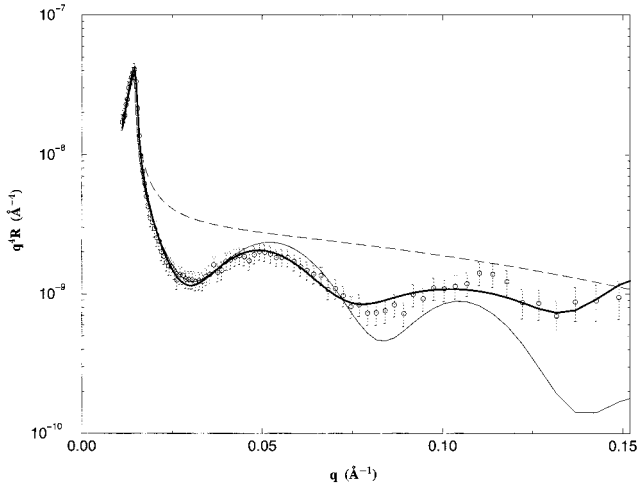

Figure 8. Reflectivity profile, q^4R vs q, and fits for the 345 K dry PMMA layer on quartz against air. The line is a single box model fit while the bold line is a refined five-box fit. The dashed line shows the clean substrate reflectivity.

Table 3. Mean Scattering Length Densities of Dry Residual Layers from Five-Box Fits

mol. weight ($\times 10^{-3}$)	β (Å^{-2} $\times$ 10^6)
13	0.66
25	0.83
70	1.15
100	1.09
216	0.92
345	0.81

dense PMMA, indicating that the layer included a substantial amount of D_2O. This supports the explanation that the 13 K layer suffered "patchy" desorption during the leaching step, leaving "holes" or "valleys" filled by the adjacent fluid medium.

3. Detailed Structure of Dry Layers. The layers characterized in Figure 7 are at the lower limit of thicknesses that can be obtained for polymers on substrates. A number of investigators have studied very thin ($h_{dry} \sim O(1 - 10R_g)$) films of PMMA[29−31] and polystyrene (PS)[32−35] on silica or oxidized silicon, prepared by spin-casting. Densities both above and below the bulk value have been reported, as well as nontrivial density profiles within the dense thin films. Although somewhat aside from the main point of this work, we carried out detailed modeling of the dry layers in Figure 7 for the molecular weight range 25 K ≤ M ≤ 345 K to compare with the prior work on very thin films.

To simulate a smooth, internal scattering length density profile within the films, we assumed a five-box model allowing variation in the scattering length density and the thickness of each box and including one adjustable roughness parameter applied to all six interfaces in the model, serving to smooth the unrealistic sharp discontinuities. The initial values of the scattering density and the total layer height were set from one-box fitting results. In every case where it was applied, the five-box model result gave significant improvement in the quality of fit over the corresponding one-box fit, as indicated by χ^2. Representative results appear in Figure 8 for $M = 345$ K. Table 3 collects the mean scattering length densities for the cases studied.

In all cases, the densities found immediately adjacent to the substrate surface are about 6−8% higher than the bulk value. This agrees with the results of Fernandez et al.,[29] who reported a modest increase in density above the bulk value in films somewhat thicker than those examined here (greater than 200 Å) of D-PMMA spin-cast and annealed on glass. However, this disagrees with Wu et al.,[31] who reported lower-than-bulk densities in thin (75−570 Å) D-PMMA films spin-cast and annealed on silicon; the difference in the latter study may be due to different surface chemistries for oxidized silicon and silica, the latter generally being more hydrophillic.

We observed for the higher molecular weights, 216 K and 345 K, a lower-than-bulk density at the free surface of the film, which led to *average* β value lower than those of bulk PMMA (see Table 3). This feature has also been observed by Fernandez et al.[29] and in Wu et al.'s[30] study of somewhat thicker (133−566 Å), spin-cast D-PMMA films on silicon, where they found a region of size ∼45 Å at the free surface of the film of density about half that of the rest of the film. The lower molecular weight films in the range considered here did not show a surface region of lower density.

C. Brushes from Melt-Adsorbed Layers. Here, we discuss experiments designed to directly interrogate the structure of an immobilized melt layer swollen in a good solvent. Recall that in the case of an equilibrated melt, Guiselin's theory gives the polymer density profile $\phi(z) \sim z^{-2/5}$ over a central portion of the profile (there are, of course, short and long length scale cutoffs, and different shapes are expected outside the cutoffs, as discussed below). A rough simulation of this situation, in Figure 3, anticipates the reflectivity profiles. The experiment demands inverted geometry (Figure 1), which requires longer counting times than for experiments against air, due to partial attenuation of the incident beam. Consequently, these experiments were time-consuming, and only two molecular weights were examined.

Figures 9a and 11a show data taken on residual layers swollen in D-benzene after annealing the melts for very long times (see Table 2); Figure 9a shows the data for $M = 174$ K while Figure 11a shows the result for $M = 520$ K. The general structure anticipated in Figure 3 is evident in both data sets. After the critical edge, one sees the onset of a broad, low-frequency fringe of high amplitude with low-amplitude, high-frequency fringes superimposed. The broad fringe presumably arises from a thin dense layer immediately adjacent to the substrate, while the high-frequency component derives from a dilute, swollen part adjacent to the solvent.

Both data sets data were fit with a two-box model, composed of a thin layer adjacent to the substrate with a low value of β, comprised mainly of PMMA, and a much thicker layer with a high β, comprised mainly of D-benzene together with a minor fraction of PMMA. Gaussian damping was applied independently to each interface in the model. The line in Figure 9a shows the two-box fit for the 174 K polymer, corresponding to the $\beta(z)$ in Figure 9b; the results for the 520 K polymer are similar. The two-box model clearly captures the main qualitative features, although the quantitative representation is poor (e.g. $\chi^2 = 14.7$ for the fit in Figure 9a). Table 4 collects the parameters from the two-box fits.

The model indicates that within 20 Å of the quartz surface the brush is very concentrated in polymer, near melt density; for example, for the 174 K material the inner layer polymer volume fraction from the fit is ≃1, while for the 520 K polymer the value spuriously

exceeds unity. The model also indicates that the outer layer is very thick and dilute; for the 174 K material, the outer layer thickness is nearly a factor of 7 greater than the coil's radius of gyration and only 4−5% polymer by volume. Although crude, the two-box model clearly indicates that a highly swollen, stretched structure results when layers adsorbed from the melt are swollen in solvent.

A much better representation of the brush data results from a fit with a power-law polymer segment density profile inspired by Guiselin's calculation, but including inner and outer cutoffs. For distances from the substrate less than some small value h_{inner}, on the order of a few Kuhn lengths, the polymer fraction is assumed to be constant at ϕ_s. Beyond h_{inner}, the polymer fraction decays by a power law, $\sim z^{-\gamma}$, which holds to an outer cutoff, h_{outer}, and then switches to exponential decay with a decay length h_{foot}:

$$\phi(z) = \begin{cases} \phi_{\text{surf}}\ (z \le h_{\text{inner}}) \\ \phi_{\text{surf}} \left(\dfrac{h_{\text{inner}}}{h_{\text{inner}} + z}\right)^{\gamma}\ (h_{\text{inner}} \le z \le h_{\text{outer}}) \\ \phi_{\text{surf}} \left(\dfrac{h_{\text{inner}}}{h_{\text{inner}} + h_{\text{outer}}}\right)^{\gamma} \exp -\left(\dfrac{z-h_{\text{outer}}}{h_{\text{foot}}}\right)\ (z > h_{\text{outer}}) \end{cases} \quad (1)$$

Gaussian damping is applied at the three interfaces, quartz, inner cutoff, and outer cutoff, with the first two assigned the same $\sigma = \sigma_{\text{substrate}}$ and the last getting an independent coefficient, σ_{outer}. One gets the scattering length density profile from

$$\beta(z) = \phi\beta_{\text{PMMA}} + (1 - \phi)\,\beta_{\text{D-benzene}} \quad (2)$$

where β_{PMMA} (=1.04 × 10^{-6} Å^{-2}) and $\beta_{D-\text{benzene}}$ (=5.4 × 10^{-6} Å^{-2}) are the scattering length densities of pure PMMA and D-benzene, respectively.

The model in eq 1 has seven parameters. To reduce the degrees of freedom, we assigned $\phi_{surf} = 1$, based on the two-box fitting of the brush data, and set $\sigma_{\text{substrate}}$ to the value from fitting of the clean substrates, leaving five adjustable parameters. The solid lines in Figures 10a and 11a show the power-law fits for the 174 K and 520 K polymers, respectively; Figures 10 and 11b show the corresponding $\beta(z)$, as discretized by the algorithm used to predict the corresponding $R(q)$. These are much better quantitative representations than the two-box fits ($\chi^2 \simeq 5$ in both cases). Table 5 collects the parameters found. Consistent with the two-box model fits, and with expectations, the inner cutoff in both cases is just a few Kuhn lengths. According to this model, the layers are indeed stretched considerably. The sum $h_{\text{foot}} + h_{\text{outer}} \equiv h_{\text{total}}$ is 1050 Å for the 174 K polymer, about $11.5R_g$, and 1880 Å for the 520 K polymer, about $12.2R_g$.

While the length scales retrieved from fits with the power-law model agree qualitatively with expectations, the results do not agree quantitatively with Guiselin's predictions. In particular, the power-law exponent γ found from the data is about double the predicted value of 2/5. The molecular implication of our observed γ value can be obtained using the scaling description of adsorbed layers by Guiselin[11] and discussed in detail in the work of Aubouy et al.[36] One can relate the important structural features of an adsorbed, swollen layer, h_{outer} and $\phi(z)$, to the single-chain loop distribution, $f(n)$, giving the number of loops per chain with n segments. Assuming no desorption results from leaching and swelling, $f(n)$ is of course the dry melt layer distribution, which for a fully equilibrated layer scales as $f(n) \sim n^{-3/2}$. If the real loop distribution is algebraic

$$f(n) \simeq N^{\alpha-1} n^{-\alpha} \qquad \alpha > 1,$$

then, assuming a densely covered surface, one finds

$$h_{\text{swollen}} \sim N^{\beta} \qquad \beta = \frac{4-\alpha}{3}$$

$$\phi(z) \sim z^{-\gamma} \qquad \gamma = 2\frac{\alpha-1}{4-\alpha}$$

We determined γ directly and so can deduce the single chain loop distribution. We find $f(n) \sim n^{-1.8}$, which decays more strongly than predicted by the reflected random-walk picture, $f(n) \sim n^{-1.5}$. The implication is that the adsorbed chains have fewer large loops than expected from random-walk statistics. This has the result of weaker scaling with molecular weight of the layer's extension, $h_{\text{swollen}} \sim N^{0.72\pm.03}$ relative to the $h_{\text{swollen}} \sim N^{5/6}$ predicted by Guiselin.

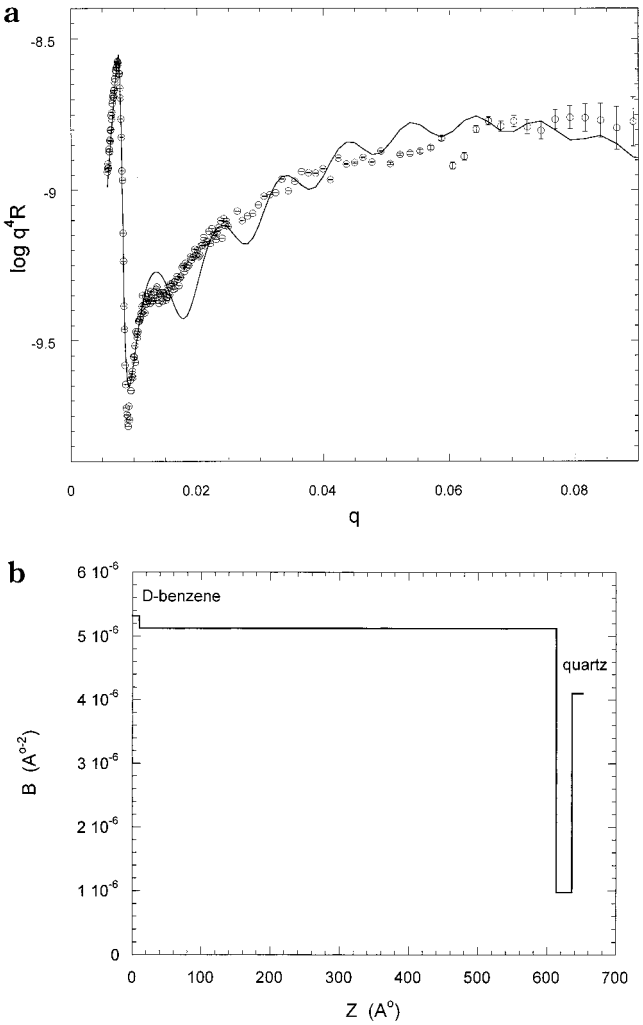

Figure 9. (a) Reflectivity profile, q^4R vs q, for the 174 K PMMA layer on single-crystal quartz swollen in D-benzene together with the two-box model fit (solid line) described in the text (b) $\beta(z)$ corresponding to Figure 9a.

IV. Summary and Conclusions

Immobilized layers of poly(methyl methacrylate) were produced by spin-coating moderately concentrated solu-

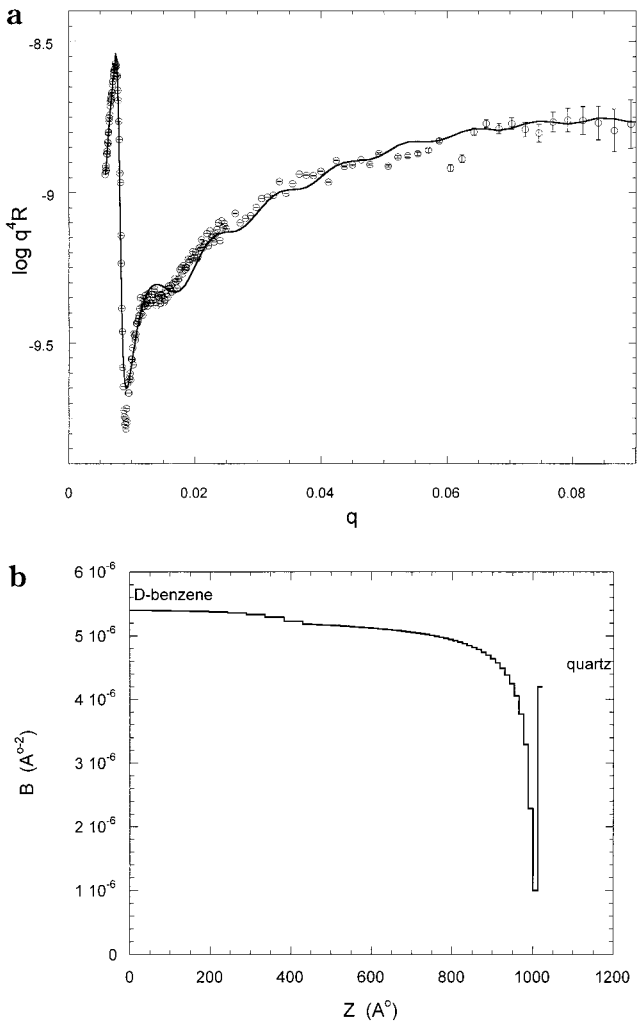

Figure 10. (a) Reflectivity profile, q^4R vs q, for the 174 K PMMA layer on single-crystal quartz swollen in D-benzene together with the constrained power-law model fit (solid line) described in the text. (b) $\beta(z)$ corresponding to Figure 10a.

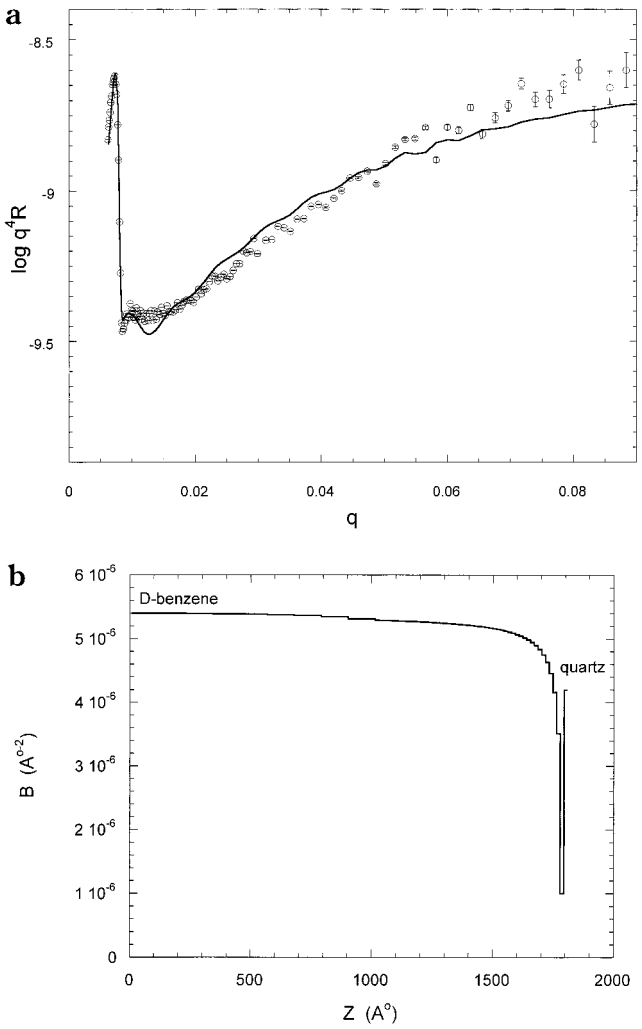

Figure 11. (a) Reflectivity profile, q^4R vs q, for the 520 K PMMA layer on single-crystal quartz swollen in D-benzene together with the constrained power-law model fit (solid line) described in the text. (b) $\beta(z)$ corresponding to Figure 11a.

tions onto hydroxylated quartz and annealing at melt conditions to erase the casting history. The annealed layers were then cooled to room temperature and unbound material was leached away in good solvent (benzene) to leave a residual, strongly adsorbed layer. The architecture of this layer was studied by neutron reflection. The effects of varying annealing time and molecular weight were studied.

The data show that spin-coating without annealing, followed by leaching in good solvent, produces thin layers, collapsed relative to those expected from "trapping" chains in the melt, with simple random-walk statistics. Annealing relaxes this initial nonequilibrium structure. After sufficiently long annealing before rinsing, the dry residual adsorbed layer thicknesses scale $h_{dry} \sim \Gamma \sim N^{0.47\pm.05}$, close to the law $h \sim N^{1/2}$, as expected from the random-walk model.

The dried adsorbed layers are the thinnest possible for this system. Those from melts equilibrated against the wall showed a "core" density adjacent to the substrate somewhat above the bulk value, in agreement with the data of Fernandez et al.[29] for somewhat thicker D-PMMA films spin-coated on glass and annealed. At the higher molecular weights, dried films exhibited depleted density at the free surface; this feature was not observed for the layers prepared from the lower molecular weight polymer (≤100 K).

Table 4. Parameters from Two-Box Fits of Swollen Layer Data

mol. weight ($\times 10^{-3}$)	β_1 (Å^{-2} × 10^6)[a]	h_1 (Å)[a]	β_2 (Å^{-2} × 10^6)[b]	h_2 (Å)[b]
174	5.2 ± .1	603 ± 6	1.1 ± 0.2	23 ± 6
520	5.3 ± .1	677 ± 8	0.8 ± 0.15	16 ± 3

[a] Subscript 1 indicates layer adjacent to D-benzene. [b] Subscript 2 indicates layer adjacent to quartz.

Table 5. Parameters from Power-Law Fits of Swollen Layer Data

mol. weight ($\times 10^{-3}$)	h_{inner} (Å)	h_{outer} (Å)	h_{foot} (Å)	σ_{outer} (Å)	γ
174	11.1 ± 0.2	582 ± 8	470 ± 48	80 ± 17	0.76 ± 0.05
520	8.3 ± 0.5	780 ± 23	1100 ± 170	110 ± 37	0.82 ± 0.02

The residual adsorbed layers swollen in good solvent exhibit a highly extended structure, consistent with a power-law profile $\phi(z) \sim z^{-\gamma}$ ($\gamma > 0$). However, values of γ determined experimentally are about double the 2/5 predicted from the loop statistics for reflected random walks. The data suggest a suppression of large loops in the adsorbed chains relative to expectation. This could be the result of not fully equilibrating the PMMA melt against the quartz substrates in the annealing step.

Indeed, computer simulations suggest that this process is logarithmically slow in later stages, so it is possible that the annealing times were just not long enough. However, this possibility does not explain why a discrepancy is not manifested in the results for dry layers, namely, the N scaling for h_{dry}. An alternative explanation which avoids this dilemma is that large loops are erased during the rinsing of unbound material from the surface.

Acknowledgment. This work was supported by the National Science Foundation under grants no. CTS 9634594 and DMR 9403566. Reflectometer beam time was provided by the Manual Lujan Jr. Neutron Scattering Center at the LANSCE Division of Los Alamos National Laboratory, Los Alamos, NM, and HFBR, Brookhaven National Laboratory, Brookhaven, NY. The Manual Lujan Jr. Neutron Scattering Center is supported by the U.S. Department of Energy under contract W-7405-ENG-36. The authors thank Prof. N. J. Turro and Dr. B. Srinivas, for valuable discussions and experimental assistance, and one of the referees, for bringing ref 15 and 16 to our attention.

References and Notes

(1) deGennes, P. G. *C. R. Acad. Sc. Paris* **1980**, *290*, 509.
(2) Silberberg, A. *J. Colloid Interface Sci.* **1981**, 90, 86; *J. Coll. Int. Sci.* **1988**, *125*, 14.
(3) By adsorbed we mean chains that have at least one segment in contact with the solid wall.
(4) The symbol ~ indicates proportionality between two quantities.
(5) Schuetjens, M. H. M.; Fleer, G. J. *J. Phys. Chem.* **1979**, 83, 1619; *J. Phys. Chem.* **1980**, *84*, 178; *Macromolecules* **1985**, *18*, 1882.
(6) Bitsanis, I. A.; ten Brinke, G. *J. Chem. Phys.* **1993**, *99*, 3100.
(7) Recently, there have been a number of careful experiments probing center-of-mass mobility of chains in the melt near a solid surface (e.g., van Alsten, J. G.; Sauer, B. B.; Walsh, D. J. *Macromolecules* **1992**, *25*, 4046.; Zheng, X.; Sauer, B. B.; van Alsten, J. G.; Schwarz, S. A.; Rafailovich, M. H.; Sokolov, J.; Rubenstein, M. *Phys. Rev. Lett.* **1995**, *74*, 407.; Lin, E.; Wu, W. L.; Satija, S. K. *Macromolecules* **1997**, *30*, 7224.). These clearly indicate severely retarded long wavelength dynamics for entangled chains near a surface.
(8) Cohen-Addad, J. P. *Polymer* **1989**, *30*, 1820.
(9) de Groot, J. V.; Macosko, C. W.; Kume, T.; Hashimoto, T. *J. Colloid Interface Sci.* **1994**, *166*, 404.
(10) Auvray, L.; Cruz, M.; Auroy, P. *J. Phys. (Fr.) II* **1992**, *2*, 1133.
(11) Guiselin, O. *Europhys. Lett.* **1992**, *17*, 225.
(12) By brushlike, we mean that lateral repulsive interactions are an important feature when the layer is swollen with good solvent. The result is a strong dependence of the swollen layer's height, $h_{swollen}$, on molecular weight, approaching $h_{swollen} \sim N$.
(13) Alexander, S. *J. Physics (Paris)* **1977**, *38*, 983.
(14) Auvray, L.; Auroy, P.; Cruz, M. *J. Phys. (Fr.) I* **1992**, *2*, 943.
(15) Cohen-Addad, J. P.; Morel, N. *C.R. Acad. Sci. II* **1995**, *320*, 455.
(16) Cohen-Addad, J. P.; Dujourdy, L. *Polym. Bull.* **1998**, *41*, 253.
(17) As a benchmark in a closely related system, Johnson and Granick (Johnson, H. E.; Granick, S. *Science* **1992**, *255*, 966, and references therein) estimated the sticking energy for the PMMA/SiO_2/CCl_4 system to be approximately $4kT$ at room temperature.
(18) An estimate of the drying time for the spin-cast film is $t_{dry} \simeq l^2/D$ where l is the spin-cast film thickness and D is the solvent diffusion coefficient in the film at the drying conditions (165 °C). Taking $l \simeq 1$ μm and $D \simeq 10^{-10}$ cm^2/s gives $t_{dry} \simeq 10^2$ s; annealing times were generally much longer than this.
(19) Iler, R. K. *The Chemistry of Silica*; Wiley: New York, 1979.
(20) Pefferkorn, E.; Haouam, A.; Varoqui, R. *Macromolecules* **1988**, *21*, 2111.
(21) Kobayashi, K.; Araki, K.; Imamura, Y. *Bull. Chem. Soc. Jpn.* **1989**, *62*, 3421.
(22) In some cases, purified nitrogen was used as the inert purge gas.
(23) Baker, S. M.; Smith, G.; Pynn, R.; Butler, P.; Hayter, J.; Hamilton, W.; Magid, L. *Rev. Sci. Instrum.* **1994**, *65*, 412.
(24) Russell, T. P. *Mater. Sci. Rep.* **1990**, *5*, 171.
(25) We used a FORTRAN program which implements Marquardt's weighted least-squares fitting (Marquardt, D. W. *J. Soc. App. Math.* **1963**, *11*, 431), giving optimal values of parameters for any assumed scattering length density profile, through the minimization of $\chi^2 = 1/(1 + n + m)(\sum_i (R_{m,i} - R_{c,i})^2/\sigma_i^2)$, where $R_{m,i}$ and $R_{c,i}$ are the measured and calculated reflectivities at q_i, respectively, σ_i^2 is the variance weighting the data point at q_i, m is the number of adjustable parameters in the model considered, and n the total number of points measured. χ^2 measures goodness of fit while weighting the error at each data point by its uncertainty.
(26) For example, for single-crystal quartz against air, $q_c = (16\pi\Delta\beta)^{1/2} = 0.0145$ Å^{-1}, where $\Delta\beta$ is the relevant β difference.
(27) Zajac, R.; Chakrabarti, A. *Phys. Rev. E* **1995**, *52*, 6536.
(28) Frank, C. W.; Rao, V.; Despotopolou, M. M.; Pease, R. F. W.; Hinsberg, W. D.; Miller, R. D.; Rabolt, J. F. *Science* **1996**, *273*, 912.
(29) Fernandez, M. L.; Higgins, J. S.; Penfold, J.; Shackleton, C. S. *Polym. Commun.* **1990**, *31*, 124.
(30) Wu, W.; Orts, W. J.; van Zanten, J. H.; Fanconi, B. M. *J. Pol. Sci. Part B: Polym. Phys.* **1994**, *32*, 2475.
(31) Wu, W.; van Zanten, J. H.; Orts, W. J. *Macromolecules* **1995**, *28*, 771.
(32) Reiter, G. *Europhys. Lett.* **1993**, *23*, 579.
(33) Keddie, J. L.; Jones, R. A. L.; Cory, R. A. *Europhys. Lett.* **1994**, *27*, 59.
(34) DeMaggio, G. B.; Frieze, W. E.; Gidley, D. W.; Zhu, M.; Hristov H. A.; Yee, A. F. *Phys, Rev. Lett.* **1997**, *78*, 1524.
(35) Forrest, J. A.; Dalnoki-Veress K.; Dutcher, J. R. *Phys. Rev. E* **1997**, *56*, 5705.
(36) Aubouy, M.; Guiselin, O.; Raphael, E. *Macromolecules* **1996**, *29*, 7261.

MA981785K